14th International Symposium
on Turbulence and
Shear Flow Phenomena (TSFP14)
July 28–31, 2026, Heidelberg, Germany

# Investigating Prandtl and Reynolds number effects on passive scalar transfer in turbulent annular pipe flow with a stochastic model

Pei-Yun Tsai [1,2], Marten Klein [1,2] and Heiko Schmidt [1,2]

[1] Chair of Numerical Fluid and Gas Dynamics, Brandenburg University of Technology, Cottbus, Germany
[2] Scientific Computing (SC) Lab, Energy Innovation Center (EIZ), Brandenburg University of Technology, Cottbus, Germany

Brandenburgische Technische Universität Cottbus - Senftenberg
Energie-Innovationszentrum Cottbus

## Introduction

### Challenges:

- **High computational cost** of conventional model (DNS/LES)
- **Curved geometry** adds complexity
- **Limited** availability of validation and experimental data
- Forward modeling of coupled turbulent heat and momentum transfer in annular pipes

### Objectives:

- Investigate **Reynolds** and **Prandtl number** dependence of the Nusselt number
- Understand the role of **spanwise curvature** on the heat transfer in annular pipe flow
- Use **One-dimensional turbulence (ODT)** as a standalone tool to simulate turbulent flow

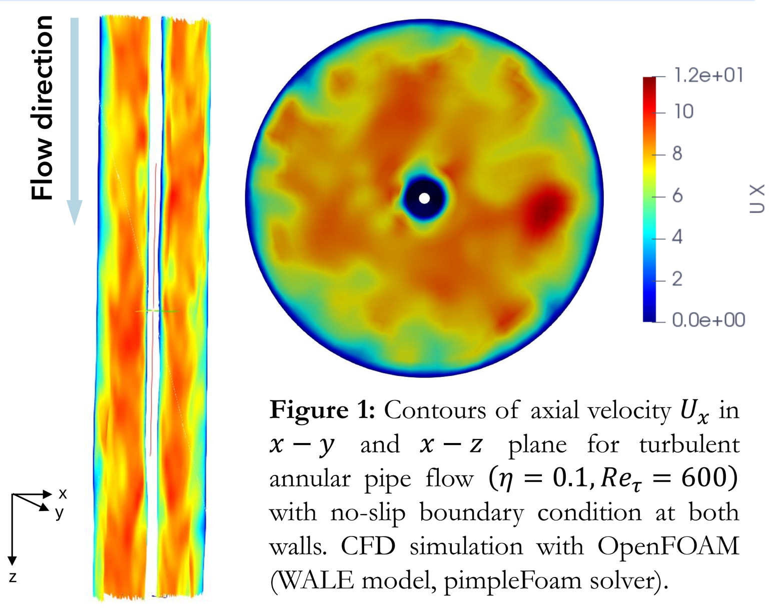


**Figure 1:** Contours of axial velocity $U_x$ in $x-y$ and $x-z$ plane for turbulent annular pipe flow ($\eta = 0.1, Re_\tau = 600$) with no-slip boundary condition at both walls. CFD simulation with OpenFOAM (WALE model, pimpleFoam solver).

## Method

One-dimensional turbulence (ODT) model [1] is a dimensionally reduced flow model that can be economically utilized as a stand-alone tool. ODT offers **full-scale resolution** of the instantaneous velocity and temperature profile along a 1D radial coordinate [2] by modeling the advection terms using a stochastic process.

Here, we consider pressure-driven (Poiseuille flow) annular pipe flow with no-slip and constant heat flux boundary conditions on the inner and outer cylindrical walls. The governing equations can be written as [3,4,5] :

$$\frac{\partial u_i}{\partial t} + \sum_{t_e} \varepsilon_u\, \delta(t-t_e) = \frac{1}{r}\frac{\partial}{\partial r}\left(r\nu\frac{\partial u_i}{\partial r}\right) - \frac{1}{\rho}\frac{dP}{dx}\delta_{1i} \quad (1)$$

$$\frac{\partial \Theta}{\partial t} + \sum_{t_e} \varepsilon_\Theta\, \delta(t-t_e) = \frac{1}{r}\frac{\partial}{\partial r}\left(r\alpha\frac{\partial \Theta}{\partial r}\right) + u\frac{d\bar{T}_w}{dx} \quad (2)$$

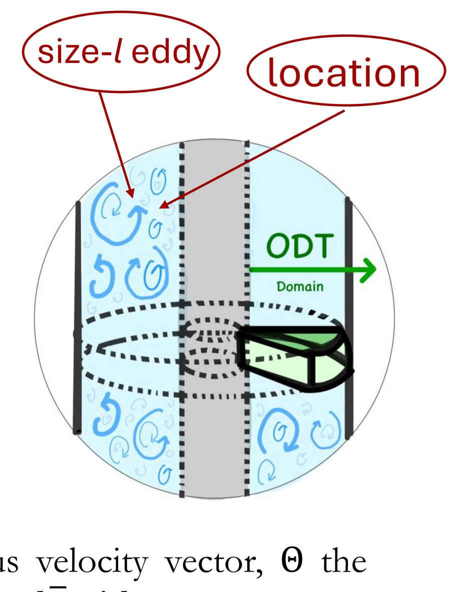


where $u_i(i = x, r, \theta)$ is the cylindrical components of the model-resolved instantaneous velocity vector, $\Theta$ the perturbation temperature relative to the axially increasing mean wall temperature $\bar{T}_w$, due to $d\bar{T}_w/dx$ is constant, $t_e$ the stochastically sampled times of eddy events affecting the velocity and scalar by $\varepsilon_u$ and $\varepsilon_\Theta$, and $\delta(t-t_e)$ is the Dirac delta function. Eddy events are modeled by spatial mappings in the form of radial 1-D.

**ODT model parameters**

- $\alpha_{ODT}$ : Energy Distribution parameter
- $C_{ODT}$ : Eddy frequency parameter
- $Z_{ODT}$ : Viscous penalty parameter

$\alpha_{ODT} = 1/6$, $C_{ODT} = 5$ and $Z_{ODT} = 400$ are used here [4]

- Eddy length: $l$
- Eddy rate: $\frac{1}{\tau} = \sqrt{\frac{1}{l^6}\left(u_K^2 + v_K^2 + w_K^2\right) - Z_{ODT}\frac{\nu^2}{l^4}}$
- Eddy rate distribution: $\lambda(l, y_0; t) = \frac{C_{ODT}}{l^2\tau(l, y_0; t)}$

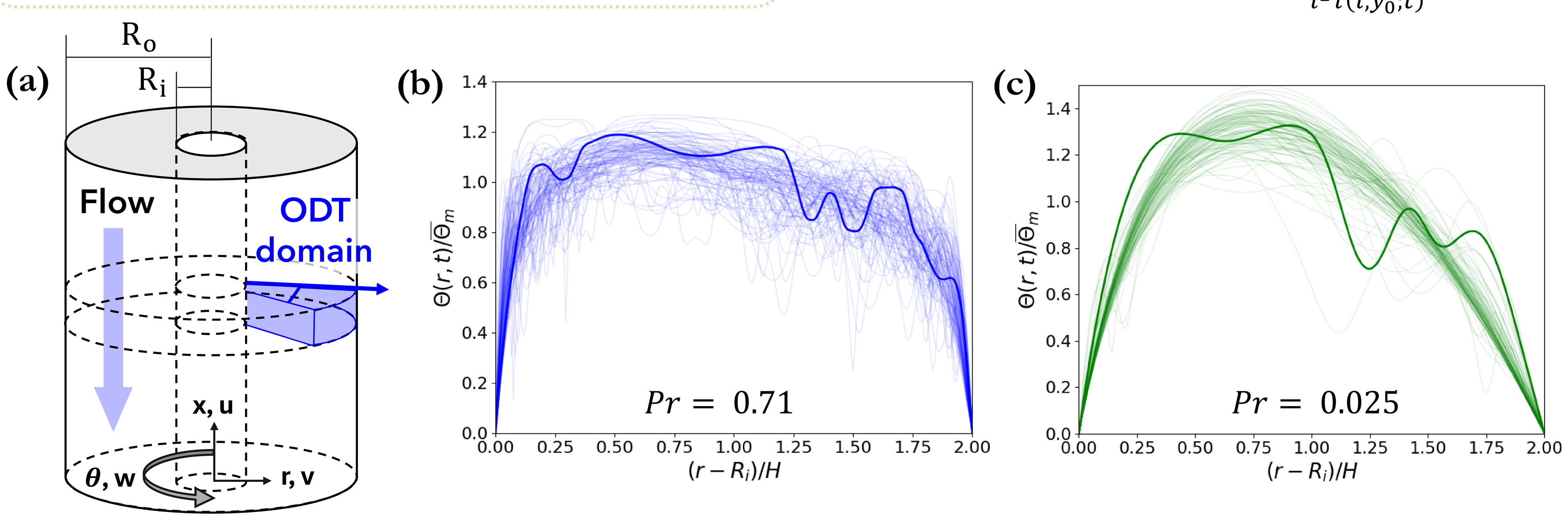


**Figure 2: (a)** Schematic of the annular pipe flow configuration with the wedge-like radially oriented ODT domain (line) is sketched. No-slip and constant heat flux boundary conditions are imposed at the annulus walls. Instantaneous temperature profiles at different simulation times for Prandtl number **(b)** $Pr = 0.71$ and **(c)** $Pr = 0.025$, bulk Reynolds number $Re_{Dh} = \frac{2(R_o - R_i)U_b}{\nu} = 1.77 \times 10^4$ and radius ratios $\eta = R_i/R_o = 0.1$ . $H = (R_o - R_i)\,/\,2$ .

## Mean temperature profile and thermal boundary layers

- **ODT accurately predicts** mean temperature profiles and the thermal law-of-the-wall for $Pr = 0.71$ .
- **Low $Pr$ (0.025)** leads to heat transfer dominated by **thermal diffusion**, with profiles close to the conductive solution.
- **Wall curvature** creates **thinner inner-wall** and **thicker outer-wall** thermal boundary layers.
- **Outer-wall profiles** follow the planar law-of-the-wall, while **inner-wall curvature** causes significant deviations.

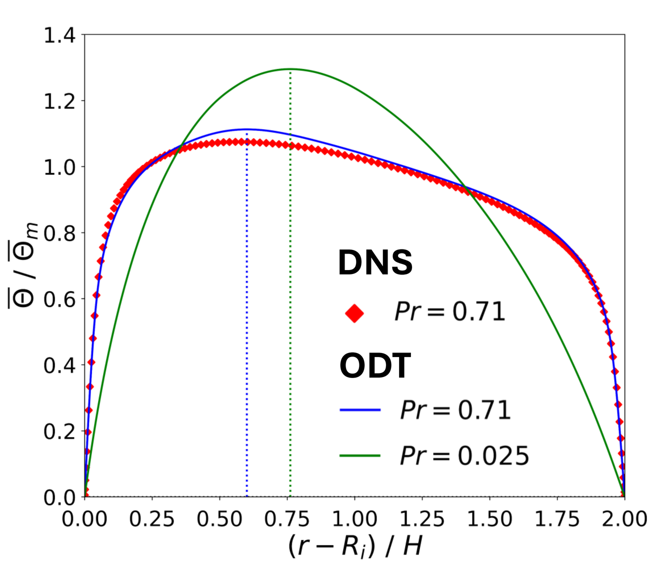


**Figure 3:** Mean perturbation temperature profiles normalized by bulk mean temperature $\bar{\Theta}_m = \frac{\int \bar{u}(r)\bar{\Theta}(r) r dr}{\int \bar{u}(r) r dr}$. Reference DNS data [5] is given.

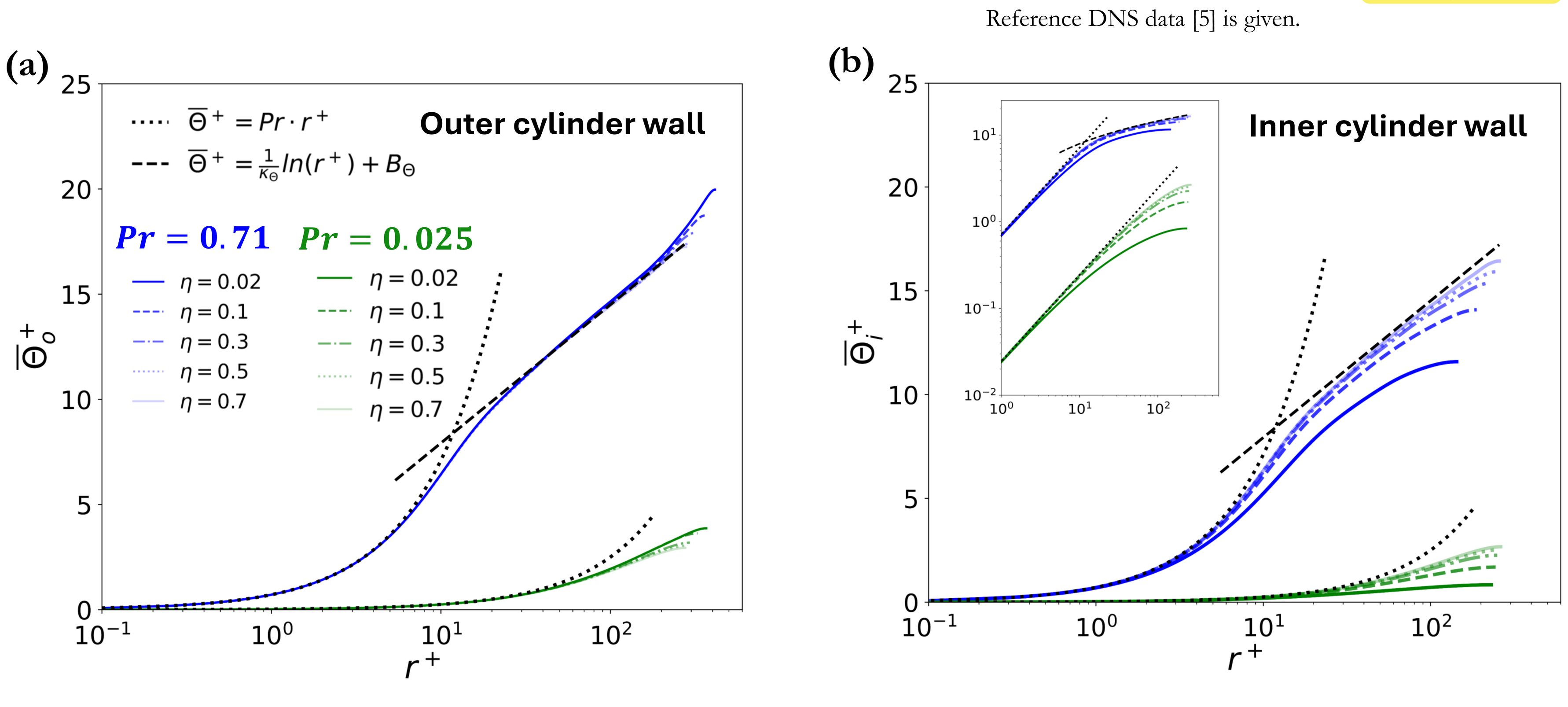


**Figure 4: (a)** Schematic Thermal boundary layer over the (a) outer and (b) inner cylinder wall for various radius ratios, $\eta = 0.02$ to 0.7, and two Prandtl numbers, $Pr = 0.71$ and 0.025, with fixed bulk Reynolds number $Re_{Dh} = 1.77 \times 10^4$.

## Nusselt number

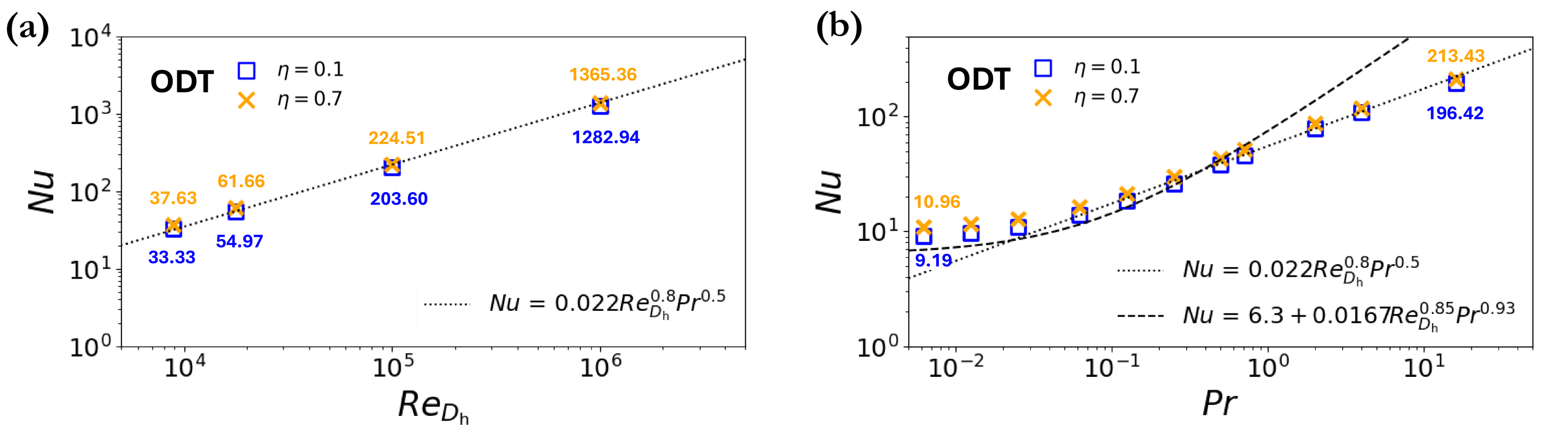


**Figure 5:** Bulk Nusselt number, $Nu \equiv \frac{\bar{q}_w}{\kappa\,\Theta_m/D_h} = \frac{4Re_\tau Pr}{\Theta_m^+}$, as a function of (a) bulk Reynolds number $Re_{Dh}$, and (b) Prandtl number $Pr$. Two radius ratios, $\eta = 0.1$ and 0.7, are shown for (a) fixed $Pr = 1$ varying $Re_{Dh}$ and in (b) fixed $Re_{Dh} = 1.77 \times 10^4$ varying $Pr$. The empirical correlation (dotted line) [6] for Prandtl numbers close to unity and another empirical correlation (dashed line) [7] for Prandtl numbers much lower than unity are given for comparison.

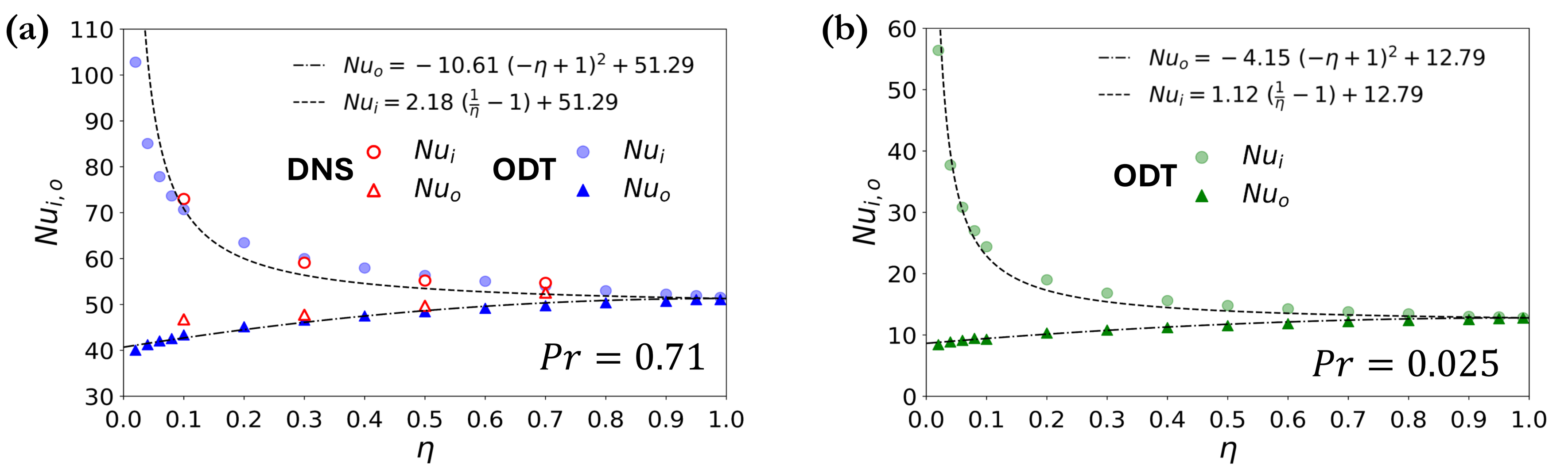


**Figure 6:** Local Nusselt number $Nu_{i/o} = \frac{D_h}{\Theta_m}\frac{\partial\bar{\Theta}}{\partial r}|_{r=R_{i/o}}$ at the cylindrical inner and outer wall, respectively, for Prandtl number (a) $Pr = 0.71$ and (b) $Pr = 0.025$, bulk Reynolds number $Re_{Dh} = 1.77 \times 10^4$ and various radius ratios $\eta$. Available reference DNS data [5] is given.

- **Bulk $Nu$ increases** monotonically with increasing $Pr$ and $Re_{Dh}$ .
- **ODT agrees well** with empirical correlations (**<5%** for high $Re_{Dh}$, **<10%** for $Pr \geq 1$).
- **$Nu$ at the inner cylinder wall** is systematically higher than at the outer wall ; the disparity increases as **$\eta$ decreases**.
- **Wall curvature** remains important even at $Re_{Dh} = 10^6$, influencing both bulk and local heat transfer.

## Boundary layer analysis

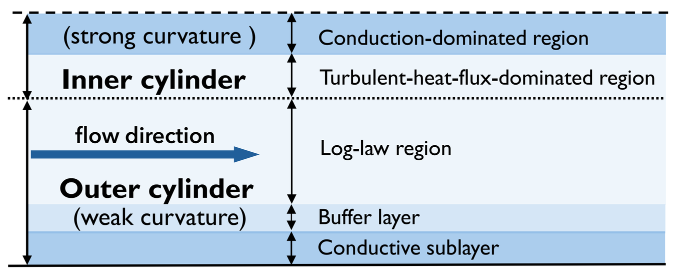


We assume that the mean flow is fully developed and axisymmetric. After applying the temporal average to the passive temperature equation (2), re-arranging, and integration over $r$, yields the turbulent heat flux balance equation as

$$\overline{\Theta' v'} - \alpha\frac{\partial\bar{\Theta}}{\partial r} = r\bar{u}\frac{d\bar{T}_w}{dx} + \frac{C_1}{r}, \text{ where } C_1 = \frac{1}{\rho C_p}\frac{q_i R_o - q_o R_i}{R_i/R_o - R_o/R_i} \quad (3)$$

### The conductive-dominated region

- In the region **very close to the inner cylinder**
- Assume that $\overline{v'\Theta'} \ll \alpha\frac{\partial\bar{\Theta}}{\partial r}$ and $R_i \ll R_o$

$$\bar{\Theta}^+(r) \approx Pr \cdot R_i^+ \ln\left(\frac{r^+ + R_i^+}{R_i^+}\right) \quad (4)$$

### The turbulent-heat-flux-dominated region

- In the region **not close to the inner cylinder**
- Assume that $\alpha\frac{\partial\bar{\Theta}}{\partial r} \ll \overline{v'\Theta'}$ and $R_i \ll R_o$
- Apply the eddy diffusivity approach $\overline{v'\Theta'} = -\alpha_t\frac{d\bar{\Theta}}{dr}$

$$\bar{\Theta}^+(r) \approx \frac{Pr_t}{\epsilon_1}\ln\left(\frac{r^+}{r^+ + R_i^+}\right) + D_1^+ \quad (5)$$

$\alpha_t = \frac{\nu_t}{Pr_t}$ with $\nu_t = \epsilon_1\sqrt{\frac{\tau_i}{\rho}}(r - R_i)$ [8]

$\epsilon_1$ and $D_1^+$ are constants, which can be obtained with least square fitting.

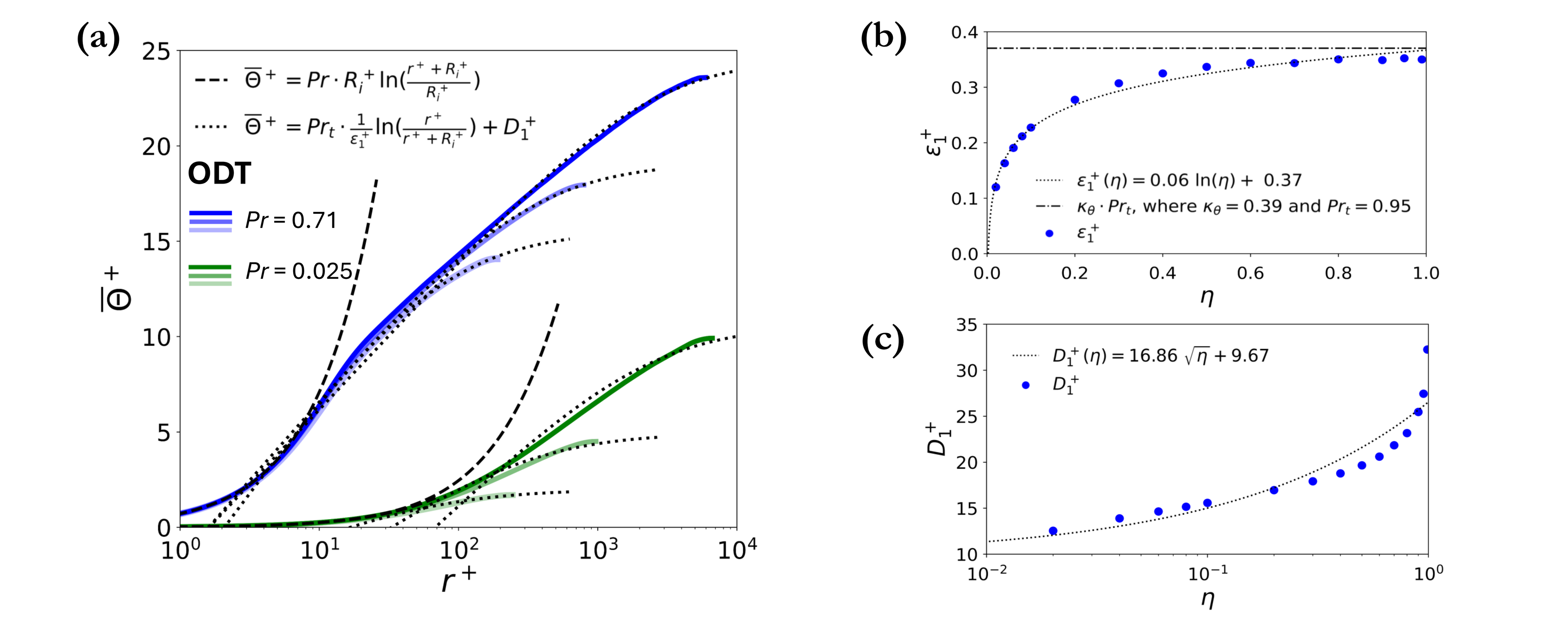


**Figure 7:** (a) Boundary layer profiles of the mean perturbation temperature over the cylindrical inner wall for $Re_{Dh} = 1.77 \times 10^4$, $10^5$ and $10^6$ (shading of lines from light to dark) investigating $Pr = 0.71$ and 0.025, respectively, for the fixed radius ratio $\eta = 0.1$ . Radius ratio dependence of the profile parameter (b) $\epsilon_1^+$ and (c) $D_1^+$ obtained by fitting the analytical expressions to the ODT simulation results in the vicinity of the cylindrical inner wall.

- **Wall-curvature coefficients** vary systematically with radius ratio $\eta$, approaching the **planar law-of-the-wall** as $\eta \to 1$.
- **Increasing $Re_{Dh}$** strengthens the logarithmic thermal layer, with a **distinct log region emerging for low Prandtl number** $Pr = 0.025$ at high Reynolds numbers.

## Acknowledgements

This research is supported by BTU Graduate Research School (Conference Travel Grant), the German Federal Government, the Federal Ministry of Research, Technology and Space and the State of Brandenburg within the framework of the joint project EIZ: Energy Innovation Center (project numbers 85056897 and 03SF0693A) with funds from the Structural Development Act (Strukturstärkungsgesetz) for coal-mining regions.

With funding from the:
Federal Ministry of Research, Technology and Space
LAND BRANDENBURG

## References

[1] A. R. Kerstein, J. Fluid Mech. **392**, 277–334 (1999).
[2] D. O. Lignell, V. B. Lansinger, J. A. Medina Méndez, M. Klein, A. R. Kerstein, H. Schmidt, M. Fistler and M. Oevermann, Theor. Comput. Fluid Dyn. **32**, 495–520 (2018).
[3] M. Klein, H. Schmidt and D. O. Lignell, Int. J. Heat Fluid Flow **93**, 108889 (2022).
[4] P. Y. Tsai, M. Klein, and H. Schmidt, Int. J. Heat Fluid Flow **119**, 110281 (2026).
[5] P. Y. Tsai, H. Schmidt, and M. Klein, arXiv:2607.09596 (2026).
[6] E. Bagheri and BC. Wang, Phys. Fluids **33**(5), 055131 (2021).
[7] W. M. Kays, M. E. Crawford, and B. Weigand, *Convective Heat and Mass Transfer*. McGRAW-HILL (1980).
[8] C. Sleicher and M. Rouse, Int. J. Heat Mass Transfer **18**(5), 677–683 (1975).
[9] B. J. Boersma and W. P. Breugem, Flow Turbul. Combust. **86**, 113–127 (2011).

Scan for the full paper